ORIGINAL PAPER

Crack propagation patterns and energy evolution rules of coal within slotting disturbed zone under various lateral pressure coefficients

Lin Bai-quan · Liu Ting · Zou Quan-le · Zhu Chuan-jie ·
Yan Fa-zhi · Zhang Zhen

Abstract Lateral pressure coefficient is an important parameter in geological engineering, and it influences significantly the damage zone around boreholes. In accordance with the fundamental principles of the Particle Flow Code (PFC), various models were established to investigate the crack propagation patterns and energy evolution rules of coal in disturbed zones of hydraulic slotting for various lateral pressure coefficients. Cracks around a slotted borehole propagate in the horizontal direction when the lateral pressure coefficient λ is less than 1, distribute uniformly when λ is equal to 1, and extend mostly in the vertical direction when λ is greater than 1. The total number of cracks increases linearly with λ. The variation in kinetic energy for coal failure was recorded; kinetic energy evolution observes a similar rule and its process can be divided into four stages, namely, the quick-release, rapid dissipation, drastic fluctuation, and stabilized stages. The peak value of the kinetic energy increases linearly with λ. The acoustic emission events distribute discretely when λ is small and uniformly when λ is equal to 1. The variation in acoustic emission events tends to increase sharply before decreasing when λ is greater than 1. The research findings are significant to the exploration of pressure relief mechanisms for hydraulic slotting from a microcosmic perspective.

Keywords Hydraulic slotting · Micro-crack · Lateral pressure coefficient · Energy evolution

L. Bai-quan · L. Ting · Z. Quan-le · Z. Chuan-jie · Y. Fa-zhi ·
Z. Zhen
School of Safety Engineering, China University of Mining and
Technology, Xuzhou, Jiangsu 221116, People's Republic of China

L. Bai-quan · L. Ting (✉) · Z. Quan-le · Z. Chuan-jie · Y. Fa-zhi ·
Z. Zhen
State Key Laboratory of Coal Resources and Safe Mining, China
University of Mining and Technology, Xuzhou 221116, People's
Republic of China
e-mail: mtkcliuting2013@163.com

Introduction

High-pressure water jet is a novel technique characterized by low heat and thermal stress, reduced vibration, no pollution, high propulsive efficiency, and good maneuverability. It has been used widely in many industries such as the airline, medical, manufacturing, food, and geotechnical engineering industries (Etchells 1997; Folkes 2009; Kahlman et al. 2001; Kim et al. 2009; Kulekci 2002; Park et al. 2005; Shanmugam et al. 2008; Tang et al. 2014). Because of its superior simple and flexible performance, the mining industry has been one of the earliest users of the water jet. Recently, the high-pressure water jet technique has been used in three main applications in coal production, namely hydraulic mining, roadway excavation, and gas pre-drainage (James 2005; Sato et al. 1986; Detournay and Peirce 2014; Lin et al. 2012; Lu et al. 2011).

Hydraulic slotting, which is based on high-pressure water jet, is an effective and reliable technology characterized by desirable artificial permeability enhancement and has been used extensively in numerous coal mines in China to improve gas pre-drainage efficiency (Lin et al. 2012; Lu et al. 2010, 2011). The application of this technique has aided in the simultaneous exploitation of coal and gas, which is a crucial component of the Chinese current energy structure (Hao et al. 2014; Ni et al. 2014; Wang et al. 2012a, 2014a, b; Yin et al. 2012). Because of the importance of this technology, extensive research has been conducted on hydraulic slotting pressure relief and permeability enhancement mechanisms over recent decades. Lin et al. (2012) examined the influence of confining pressure on coal physical properties around slotted boreholes using FLAC3D software. Lu et al. (2010) proposed a new technique using high-pressure pulsed water jet to drill boreholes in stiff layers of roofs or floors based on an analysis of borehole collapse and the pore formation mechanism in stiff layers. A new water jet rotary cutting system was developed by Lu et al. to enhance coal seam permeability by creating artificial cracks. Its application showed

that the methane drainage efficiency improves three to six times compared with the traditional method (Lu et al. 2011, 2013). Song and Lu et al. analyzed the feasibility of water jet cutting technology applications in rock burst prevention using ABAQUS software and found that stress and energy can be released near the slots (Lu et al. 2011; Song et al. 2014).

From this analysis, it is obvious that research to date has tended to focus on the effect of hydraulic slotting on coal mechanical and seepage behaviors around slots from a perspective of stress, water jet impact property, and flow characteristics of depressurized gas, but limited attention has been given to crack propagation patterns and rules of energy evolution around slotted boreholes for different lateral pressure coefficients (λ). However, distinct application effects have been found in coal mines with different lateral pressure coefficients. Therefore, an exploration of the influence of lateral pressure coefficients on crack propagation patterns and energy evolution rules around slotted boreholes would be of significance.

It is difficult to study crack propagation and energy evolution in laboratory or field tests because of its high cost, inconvenience, and low accuracy (Cai et al. 2007; Damjanac et al. 2007; Yoon et al. 2014). Fortunately, numerical simulation applications are increasing rapidly because of their many advantages over the limit equilibrium method, which can be used to solve these problems. Conventional numerical methods, such as the boundary element, finite different, and finite element methods, have been used extensively to obtain stress and displacement distributions around boreholes, but the damage zones and crack propagation cannot be determined by these methods (Cai et al. 2007; Mayoral 2014; Iuspa et al. 2015; Lin et al. 2012; Li et al. 2014). Particle Flow Code (PFC), which is based on the discrete element method (DEM), can be applied to simulate the stress distribution, crack propagation, and energy evolution around a borehole because of its superiority in solving large deformation problems of solid mechanics (Cho et al. 2007; Cundall and Strack 1979; Damjanac et al. 2007; Shimizu et al. 2011a, b; Michael and Daniel 2010; Yoon et al. 2014; Potyondy and Cundall 2004; Potyondy 2007; Itasca 2004). Therefore, PFC is the preferred tool in this study.

In this study, we discuss the influence of lateral pressure coefficient on crack propagation patterns around a slotted borehole using PFC2D. The theoretical calculations are used to verify the numerical results. Finally, energy evolution around the slotted borehole is explored, which can also be applied to validate the rationality of the conclusions.

Fundamentals of hydraulic slotting

In the recent years, hydraulic slotting has played an important role in gas drainage and the elimination of coal and gas outburst in coal mines (Lu et al. 2010, 2011; Shen et al. 2012). The self-

developed high-pressure water jet slotting system is shown in Fig. 1. The system composition and functional description of the major components are listed in Table 1.

In general, hydraulic slotting procedures can be summarized as two parts: the formation of a high-pressure water jet and slotting. As depicted in Fig. 1, water that is pressurized using an emulsification pump flows into the dual-power drill bit through the control valve, sealing rotator, and drill pipe to form a high-pressure water jet. Generally, the sequences of slotting depicted in Fig. 2 can be divided into three parts: (1) drill a borehole using a low pressure water jet; (2) rotate the drill pipe and the pressurized water impacts the coal mass; and (3) haul the drill pipe towards the orifice and slot the coal seam. During hydraulic slotting, the high-pressure water jet impacts the coal mass, which results in damage to the coal mass and crack initiation. It is necessary to introduce the action mechanism of high-pressure water jets on coal mass. The evolution of water pressure during hydraulic slotting is therefore displayed in Fig. 3 based on the assumption that the water load distributes uniformly around the borehole wall during the process. At the initial time, the water pressure R_0, which is consistent with the field experiments, remains a constant 30 MPa for 1 μs. The pressure then begins to decay linearly and achieves a value of $R_1=3$ MPa at $t_2=5$ μs. From 5 to 30 μs (t_2–t_3), the pressure is maintained as R_1. Finally, it decreases to 0 at $t_4=33$ μs (Liang 2007).

The stress around the borehole changes after slotting. Cracks initiated during hydraulic slotting start to propagate around the slotted borehole by stress redistribution, which results in an enhancement of coal mass permeability and an improvement in gas drainage efficiency (Wang et al. 2012b, 2013; Ye et al. 2014; Wu et al. 2010; Zou et al. 2014a, b). The mechanism and pattern of crack propagation around the slotted borehole are unclear. The manner in which stress transfers and the patterns in which cracks propagate are related closely to the lateral pressure coefficient (Deng et al. 2014; Li et al. 2014; Zhu et al. 2013, 2014). Therefore, crack propagation patterns and energy evolution rules of coal in the slotting-disturbed zone for various lateral pressure coefficients will be elaborated upon below.

Simulation mechanism of PFC

Bond models in PFC

PFC models the movement and interaction of circular particles using the DEM, as described by Cundall and Strack (Cundall and Strack 1979). The calculation cycle in the PFC is a time-stepping algorithm that requires the repeated application of laws of motion for each particle and a force-displacement law for each contact (Al-Busaida et al. 2005). Two basic bond models are contained in the PFC: the contact and parallel bond models (CB and PB, respectively). In the CB model, the contact stiffness remains even after bond breakage as long as

Fig. 1 The indigenous hydraulic slotting system (the *red arrow* represents the flow direction of the high pressure water; the *black arrow* points to the physical figure of the components; and the *blue arrow* leads to the transverse section along line AB)
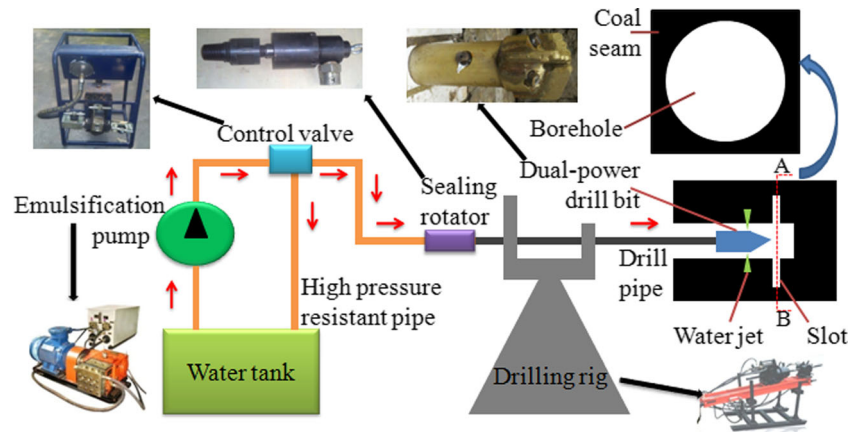
the particles remain in contact. This implies that in the CB model, if the particle contact model is maintained, bond breakage may not affect the macrostiffness significantly, which is unlikely in rocks. Contact and bond stiffness contribute in the PB model. Thus, bond breakage in the PB model results in an immediate stiffness reduction, which not only affects the stiffness of adjacent assemblies but also the macrostiffness of particle assemblies (Cho et al. 2007; Wang et al. 2014c). When particles separate, bond breakage has occurred and when they overlap, bond deformation occurs. The PB model is therefore more realistic for rock-like materials.

The mesoscopic parameters of PB strength include mainly normal strength σ_{cn}, shear strength τ_{cs}, and friction coefficient μ among particles. The prerequisite for parallel bond breakage is:

$$\sigma_{n\max} > \sigma_{cn}, \tau_{s\max} > \tau_{cs} \tag{1}$$

where $\sigma_{n\max}$ and $\tau_{s\max}$ are the maximum normal and shear stress applied to the bond, respectively.

Calibration of mesoscopic parameters in PFC

A proper selection of mesomechanical parameters is critical for simulation by PFC. Calibration of the mesoparameters to match the macroresponse is a trial and error process (Wang

et al. 2014c; Li et al. 2014). A series of tests were conducted based on macroparameters of coal in the Yangliu Mine in China (see Fig. 4). The uniaxial compression test model is 100 mm high and 50 mm wide and that in the Brazilian disc test is 50 mm in diameter (Wang et al. 2014c). The mechanical parameters of the laboratory experiment and the numerical test are shown in Table 2. The calibrated mesoscopic parameters are presented in Table 3. The macroscopic tensile strength obtained in the subsequent Brazilian test is 0.95 MPa.

**Numerical simulation results and discussions**

Numerical model

A 12×12 m square model (Fig. 5) was developed with 25,000 particles whose mesoproperties are presented in Table 3. The model is surrounded by four confining walls. The lower wall is fixed and the upper and lateral walls can move to apply constant confining pressures. Two confining pressures of 6 MPa in the y-direction and $6 \times \lambda$ MPa in the x-direction were applied to the coal mass model. For simplicity, the slotted borehole can be substituted equivalently with a borehole of 0.5 m diameter.

Table 1 Composition of the system and function description of the major components

Major components	Function
Water tank	Water supply
Emulsification pump	Power supply
Control valve	Water pressure adjustment
Sealing rotator	Connect high pressure resistant pipe with drill pipe
High pressure resistant hose	Water transport
Dual-power drill bit	Drilling and slotting
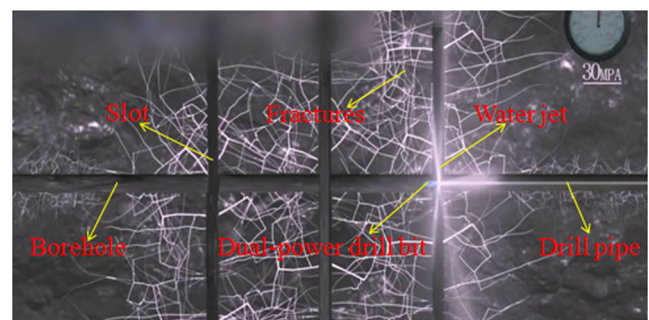
Fig. 2 The sequences of slotting (the *white polygonal lines* represent the fractures around the slotted borehole; the *black area* stands for the coal mass)
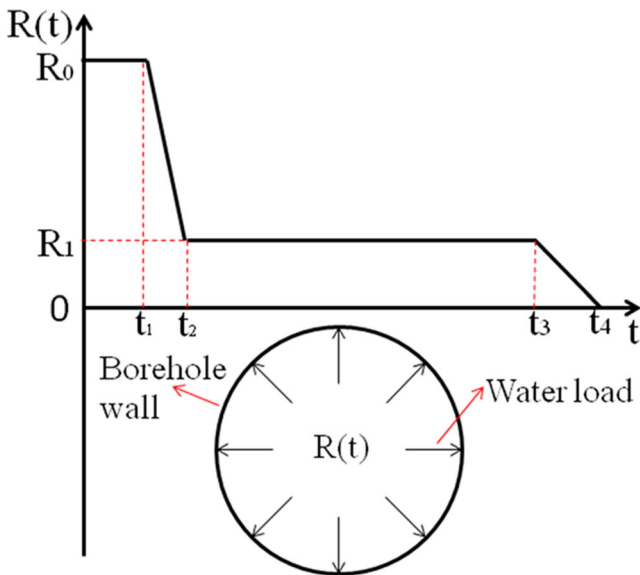
Fig. 3 The evolution of water pressure during hydraulic slotting (the *circle* in the figure represents slotted borehole; the *black arrow* in the circle points to water load)

Crack propagation patterns around the slotted borehole under different λ

Generally, it is acknowledged that the stress of the coal mass in the horizontal direction is not equal to that in the vertical direction. For example, the lateral pressure coefficients in the Huainan coal mine area in China vary from 0.49 to 1.49, and based on 116 global field data points, the stress in the horizontal direction is 0.5–2 times that in the vertical direction (Wang and Pan 2010). Thirteen lateral pressure coefficients, namely 0.5, 0.6, 0.7, 0.8, 0.9, 1.0, 1.2, 1.4, 1.5, 1.6, 1.7, 1.8, and 2.0, have been set to explain the crack propagation patterns around the slotted borehole.

Distribution of stress around the slotted borehole under various λ

After hydraulic slotting, the original stress equilibrium is broken, which results in a stress redistribution. During the

process of establishing a new balance, the loading and unloading states determine the failure patterns around the borehole (Michael and Daniel 2010; Kekec et al. 2014). Considering the above reasons, it is necessary to study the stress redistribution before exploring the crack propagation patterns around the slotted borehole.

The particle contact force distribution around the slotted borehole after equilibrium is shown in Fig. 6. When λ=0.6, the stress concentration is not obvious compared with other situations for lower stress in the horizontal direction. While λ=1.0, the stress concentration is distributed uniformly. When λ=1.8, the stress concentration is located predominantly in the vertical direction. The stress concentration becomes more obvious with an increase in λ. Similar conclusions can be obtained by analyzing the other models. In summary, if λ≠1, the stress concentration emerges in the direction of minimum principal stress. When λ=1.0, the stress concentration around the slotted borehole is distributed uniformly.

The distributions of normal bond force among particles around the slotted borehole under various lateral pressure coefficients are shown in Fig. 7. The blue zone represents the tensile stress and the red zone refers to the compressive stress. The compressive and tensile stresses are characterized by partition distribution. For λ<1.0, the compressive stress is distributed mainly in the horizontal direction, and the tensile stress is located in the vertical direction. When λ=1.0, the compressive and tensile stress distributions are uniform around the borehole. For λ>1.0, the compressive and tensile stresses concentrate in the vertical and horizontal directions, respectively. Therefore, conclusions can be drawn that the compressive stress is distributed primarily in the direction of the minimum principal stress, the tensile stress is concentrated mainly in the direction of the maximum principal stress, and the distribution range of these two stresses extends with increase in λ.

Crack propagation of coal around the slotted borehole under different λ

The crack distribution around the borehole, after a new equilibrium has been established, is illustrated in Fig. 8. When λ<1.0,

Fig. 4 Simulated PFC2D failure during a uniaxial compression test and a Brazilian disc test (the *black lines* in the figure represent cracks)
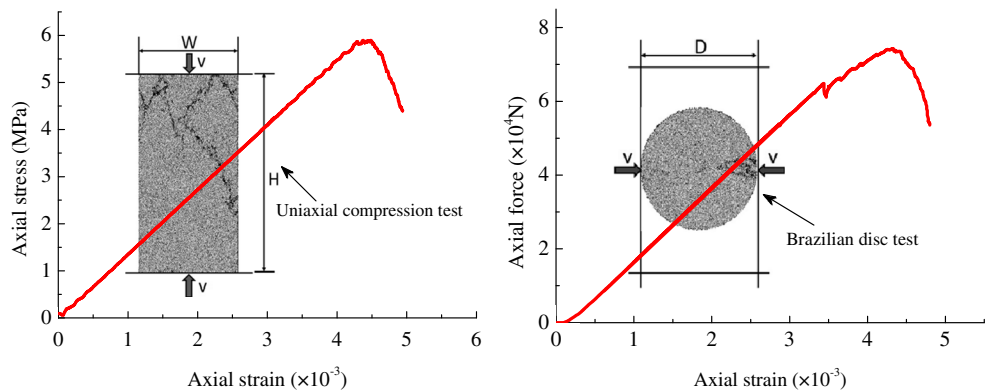
Table 2 Mechanical parameters of the laboratory experiment and numerical test

Mechanical parameters	UCS (MPa)	Elastic modulus (GPa)	Poisson's ratio
Parameters of laboratory experiments	5.81	1.28	0.23
Numerical test results	5.90	1.37	0.19
Errors (±%)	1.55	7.03	17.39

cracks propagate mainly in the horizontal direction, a few propagate in the vertical direction and the damage zone can be viewed approximately as an ellipse with a long axis in the horizontal direction. When $\lambda=1.0$, the fracture zone is almost circular. For $\lambda>1.0$, cracks concentrate mainly in the vertical direction, and the cracked zone can be considered to be an ellipse with long axis in the vertical direction.

From the compressive and tensile stress distribution laws in Fig. 7, it can be concluded that the failure zone around the borehole in the maximum principal stress orientation results from the compressive stress. This means that the cracks in this zone are compressive cracks, and that the tensile stress contributes to the damage zone in the minimum principal stress direction, which is composed of tensile cracks. The cracks generated by compressive stress in PFC can be viewed as tensile cracks. This will be explained in Section 4.2.3.

The damage zone expands with increasing λ, and the quantitative relationship between the number of cracks and λ is shown in Fig. 9. For an increase in λ, the number of cracks increases almost linearly and the damage zone expands rapidly. When λ is small, only part of the coal mass separates from the borehole wall. For a large λ, the borehole collapses. The reason for this phenomenon is that the increase in λ makes the stress concentration more obvious and leads to further bond breakage among particles, which enlarges the cracked zone.

Crack propagation patterns of slotting disturbed zone

Based on the PFC basic principles, simplified models (Fig. 10) of unloading deformation and stress distribution of particles around the slotted borehole have been established to analyze the crack propagation patterns and mechanisms. The black areas in Fig. 10 represent the overlap among particles. Larger overlapped areas imply that a stronger force

exists among particles, and that the stress concentration is greater.

By comparing Figs. 7 and 8, we see that the direction of crack propagation is approximately in accordance with the compressive stress direction, which implies that the compressive stress is the main contributor to crack propagation around the slotted borehole. Therefore, the mechanism for compression-induced crack formation in PFC should be analyzed before interpreting the crack propagation patterns around the slotted borehole. Figure 11a and b is the bond models in PFC and real rock, respectively. In Fig. 11a and b, particles 1 and 2 are bound whereas particles 3 and 4 are unbound. If the stress in the vertical direction is greater than that in the horizontal direction, the restraining bond is compressed and bond breakage will not occur. When the stress in the vertical direction is smaller than that in horizontal direction, the bond is tensed, and when the bond strength is exceeded by the tensile stress, a microcrack forms.

In Fig. 10, when $\lambda<1$, the stress in the vertical direction around the slotted borehole is greater than that in the horizontal direction (Li et al. 2013; Zhu et al. 2013), which causes tension in the vertical direction and compression in the horizontal direction. This results in a further pressure relief zone in the vertical direction and a stress concentration zone in the horizontal direction. According to the mechanism for the formation of compression-induced cracks in the PFC mentioned above, when the bond strength among particles is exceeded by the stress in the stress concentration zone, the bond breaks, and a microcrack is generated. This leads to a redistribution of local stress and forms a macro damage zone. These are the reasons for the stress distributions in Fig. 7 and the crack propagation patterns in Fig. 8. The reasons for the condition for $\lambda>1$ are similar to those depicted above. If $\lambda=1$, the stress around the slotted borehole is uniform, and the stress concentration and damage zones are approximately circular.

Table 3 The mesoscopic parameters of the PFC model

Particle basic parameters		Parallel bond parameter	
Particle density ρ (kg/m^3)	1450	Mean normal strength $\overline{\sigma}$ (MPa)	4
Minimum radii $r_{\min}$	2×10^{-4}	Standard deviation of normal strength $\overline{\sigma_s}$ (MPa)	0.1
Ball size ratio $r_{\max}/r_{\min}$	1.66	Mean shear strength $\overline{\tau}$ (MPa)	4
Particle contact modulus $\bar{E}$ (GPa)	0.8	Standard deviation of shear strength $\overline{\tau_s}$ (MPa)	0.1
Stiffness ratio k_n/k_s	1	Elastic modulus $\overline{E_c}$ (GPa)	0.8
Friction coefficient μ	0.4	Stiffness ratio $\overline{k_n/k_s}$	1
Damping constant α	0.7		
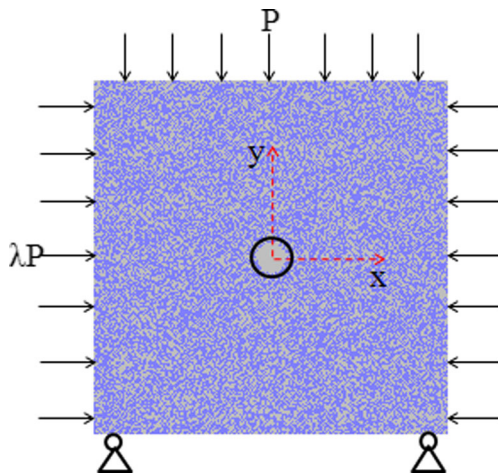
Fig. 5 Computational model (the *blue particles* compose the coal mass; the *circle* represents the slotted borehole; the *red dash arrow* points to the *x*-direction and *y*-direction; and the *black arrow* stands for the load applied to the model)

Theoretical verification of the numerical results

To theorize the reasonability of the numerical simulation results, a model of a circle in an infinite plate in a linear elastic coal mass (Fig. 12) is introduced to obtain the rules of crack distribution around the slotted borehole for various lateral pressure coefficients. The stress distribution around the circular hole can be expressed as:

$$\begin{cases} \sigma_r = \dfrac{P}{2}(1+\lambda)\left(1-\dfrac{a^2}{r^2}\right) - \dfrac{P}{2}(1-\lambda)\left(1-4\dfrac{a^2}{r^2}+3\dfrac{a^4}{r^4}\right)\cos 2\theta \\[2mm] \sigma_\theta = \dfrac{P}{2}(1+\lambda)\left(1+\dfrac{a^2}{r^2}\right) + \dfrac{P}{2}(1-\lambda)\left(1+3\dfrac{a^4}{r^4}\right)\cos 2\theta \\[2mm] \tau_{r\theta} = \dfrac{P}{2}(1-\lambda)\left(1+2\dfrac{a^2}{r^2}-3\dfrac{a^4}{r^4}\right)\sin 2\theta \end{cases}$$

$$(2)$$

where σ_r is the residual stress of the coal at any point, σ_θ is the tangential stress of the rock at any point, $\tau_{r\theta}$ is the shear stress of the rock at any point, P is the in situ stress, a is radius of the circular, and λ is the lateral pressure coefficient.

The formation of cracks in the PFC should meet the condition that the normal strength σ_{cn} of the bond between particles is exceeded by the normal stress, or the tangential strength τ_{cs} is exceeded by the shear stress (Itasca 2004). The distribution range of cracks around the borehole can be acquired as follows:

$$\{\sigma_r > \sigma_{cn}\} \cup \{\sigma_\theta > \sigma_{cn}\} \cup \{\tau_{r\theta} > \tau_{cs}\} \tag{3}$$

To analyze the distribution range of cracks around the borehole, we take $\sigma_\theta > \sigma_{cn}$ for example. It is assumed that σ_θ is equal to σ_{cn} in the border of the damage zone. Therefore, an equation can be derived as follows:

$$\frac{P}{2}(1+\lambda)\left(1+\frac{a^2}{r^2}\right) + \frac{P}{2}(1-\lambda)\left(1+3\frac{a^4}{r^4}\right)\cos 2\theta = \sigma_{cn} \tag{4}$$

if $\theta=0$, then $\sigma_\theta=(3-\lambda)P$, and while $\theta=\frac{\pi}{2}$, $\sigma_\theta=(3\lambda-1)P$.

According to the above equations, the damage zone around the borehole for various lateral pressure coefficients can be obtained as follows, with the schematic diagram shown in Fig. 13:

(1) If $\lambda=1$, Eq. (4) can be changed to $P\left(1+\frac{a^2}{r^2}\right) = \sigma_{cn}$, and the crack range can be a circle with radius $\sqrt{\frac{P}{\sigma_{cn}-P}}a$.

(2) When $\lambda>1$, the stress in the vertical direction of the borehole is greater than that in the horizontal direction. According to Eq. (4), the range of cracks in the vertical direction is larger than that in the horizontal direction and it can be approximated as an ellipse, with the long axis in the vertical direction.

| λ=0.6 | λ=1.0 | λ=1.8 |
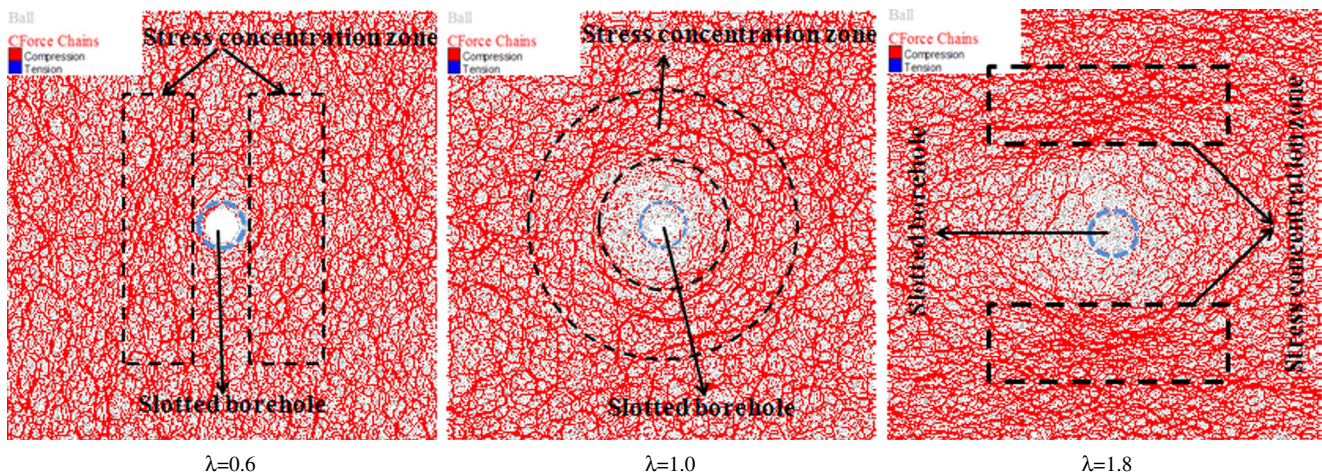
Fig. 6 Distribution of contact forces of particles around the slotted borehole (the *red curve* represents the contact force; the *blue circle* stands for the slotted borehole; and the *black circle* means the stress concentration zone)
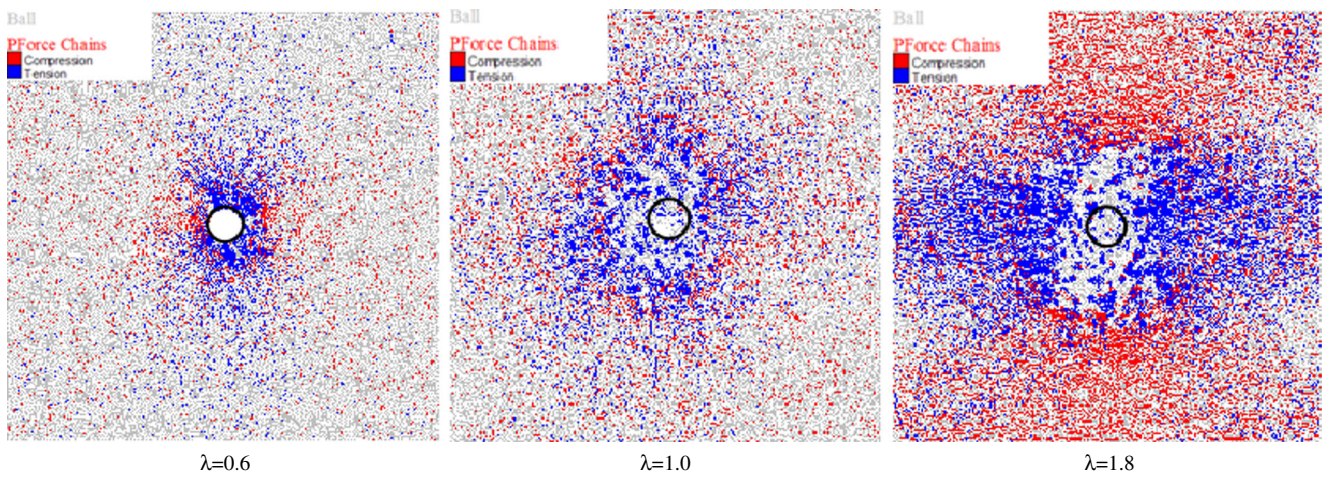
Fig. 7 Distribution of normal bond forces of particles around drill (the *black circle* represents the slotted borehole; the *blue line* means the tensile stress; the *red line* stands for the compressive stress)

(3) For $\lambda < 1$, the stress in the vertical direction of the borehole is less than that in the horizontal direction. According to Eq. (4), the crack distribution in the vertical direction has a smaller range than that in the horizontal direction and it is said to be approximately elliptical with the long axis in the horizontal direction.

The numerical conclusions were consistent with the theoretical results. Therefore, we can conclude that the conclusions are reasonable.

Rules of energy evolution around the slotted borehole under various λ

The in situ stress formed after loading is applied to the model, and energy is stored in the bond among particles in the form of strain energy. After excavation, particles move to a new space and the strain energy is converted into kinetic energy. For translational and rotational movements, the total energy of all particles in PFC motion can be expressed as (Itasca 2004):
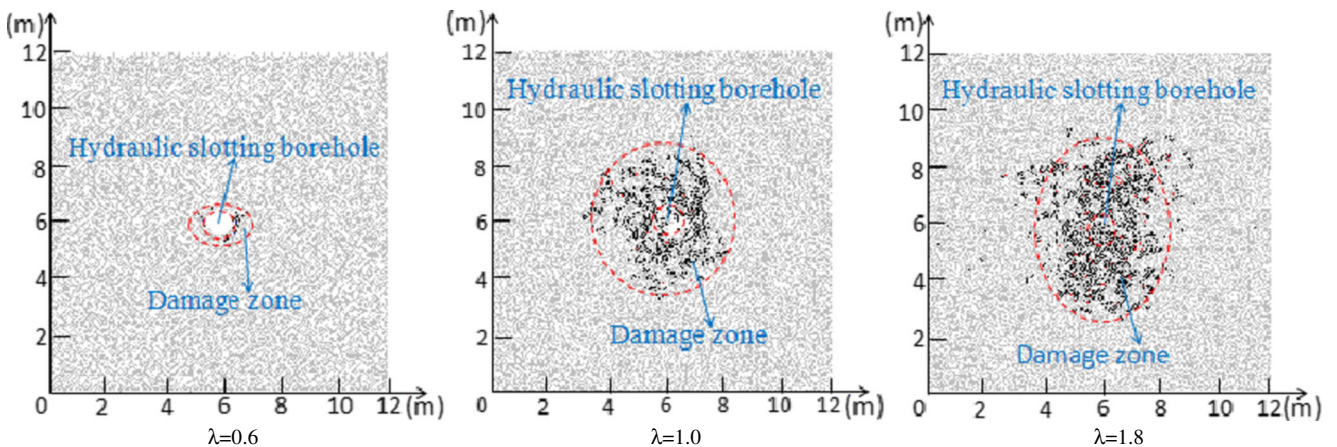
$$E_k = \frac{1}{2} \sum_{N_P} \sum_{i=1}^{3} M_{(i)} v_{(i)}^2 \tag{5}$$

where N_P is the total number of particles and $M_{(i)}$ and $v_{(i)}$ are the generalized mass and velocity, respectively, and can be obtained from Eqs. (6) and (7):
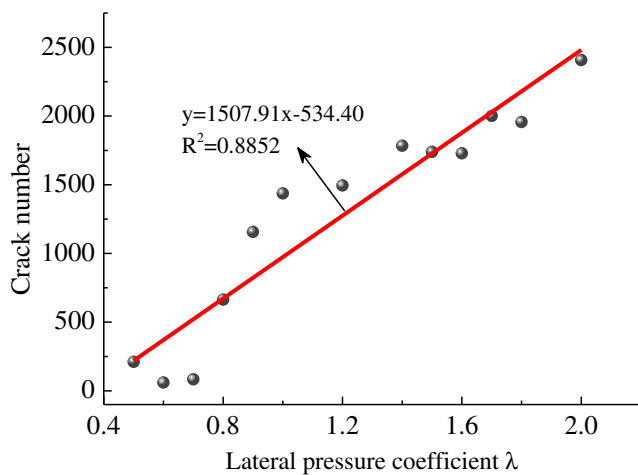
$$M_{(i)} = \begin{cases} m & (i = 1, 2) \\ I & (i = 3) \end{cases} \tag{6}$$

$$v_{(i)} = \begin{cases} \dot{x}_{(i)} & (i = 1, 2) \\ \omega_{(i)} & (i = 3) \end{cases} \tag{7}$$

where m, I, $\dot{x}_{(i)}$, and $\omega_{(i)}$ are mass, moment of inertia, translational velocity, and rotational velocity of particles, respectively.

Fig. 8 Crack distribution around drill with different lateral pressure coefficient (the *black line* means the crack)
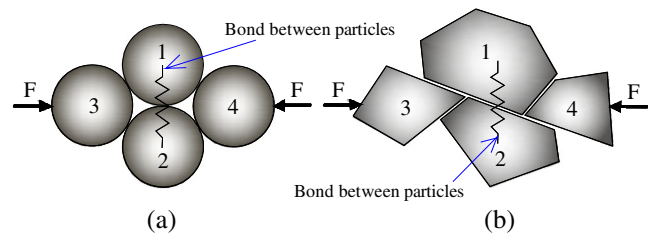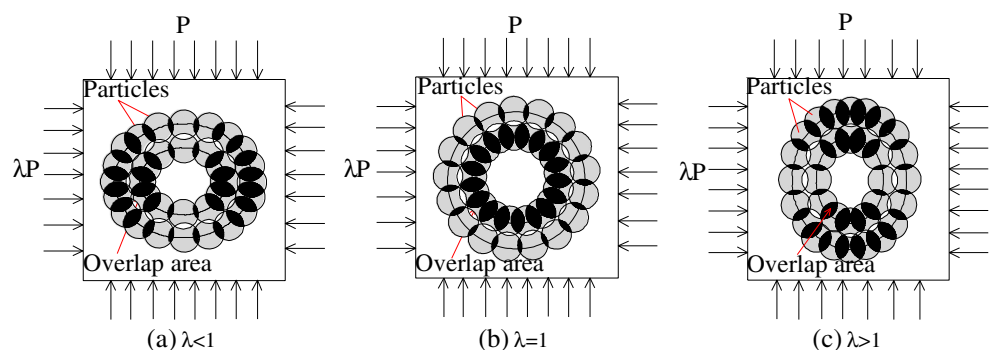
Fig. 9 Relationship between crack number and lateral pressure coefficient

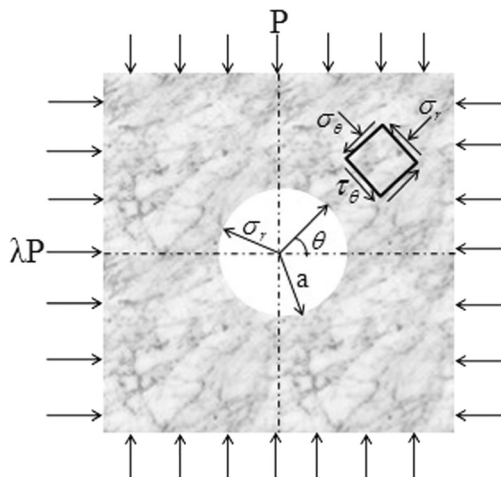Fig. 11 Mechanism for compression-induced tensile cracking (**a** model in PFC; **b** model of the real rock)

(3) Drastic fluctuation stage: numerous cracks still form during this stage and the kinetic energy is maintained at a high level. Some of the particles that became separated in the former stage come into contact with each other again, and the system is in a state of dynamic balance. This stage lasts from 0.227 to 0.6 s.

(4) Stabilized stage: when the calculation time exceeds 0.6 s, few cracks are produced. The kinetic energy is maintained at a low level and the models reach equilibrium.

The kinetic energy evolution with different lateral pressure coefficients after hydraulic slotting is shown in Fig. 14. In the entire process, the kinetic energy evolution for various λ follows a similar rule and the time history curve of kinetic energy variation can be divided into four stages: namely, the quick release, rapid dissipation, drastic fluctuation, and stabilized stages.

(1) Quick release stage: before excavation, the energy in the system is stored in the form of strain energy. Bond breakage occurs and the particles move to a new space with the redistribution of local stress after excavation. The energy stored in the system is released in the form of kinetic energy, resulting in a sharp increase in kinetic energy, which reaches a peak value in ~0.002 s at this stage.

(2) Rapid dissipation stage: particles separated for bond breakage in the first stage will come into contact with each other again and lead to an attenuation of particle velocity, and the kinetic energy in the system will transform into strain energy again. This stage lasts for ~0.225 s.

Another interesting phenomenon found from Figs. 14 and 15 is that the peak value of the kinetic energy is directly proportional to the lateral pressure coefficient, and the relationship between the two parameters shows good linearity. With an increase in λ, the kinetic energy in the system increases. The stress redistribution around the borehole is extensive and further bond breakage occurs. Consequently, the damage zone around the drill is enlarged. These occurrences verify the correctness of the conclusions mentioned above from an energy perspective.

The acoustic emission (AE) characteristics of coal are related closely to the formation of microcracks. In PFC, the formation of a microcrack is accompanied by a release of strain energy, which causes an AE event. The AE characteristics can be simulated from the statistics of microcrack number over a certain interval during loading (Cai et al. 2007; Shimizu et al. 2011a, b; Yoon et al. 2014).
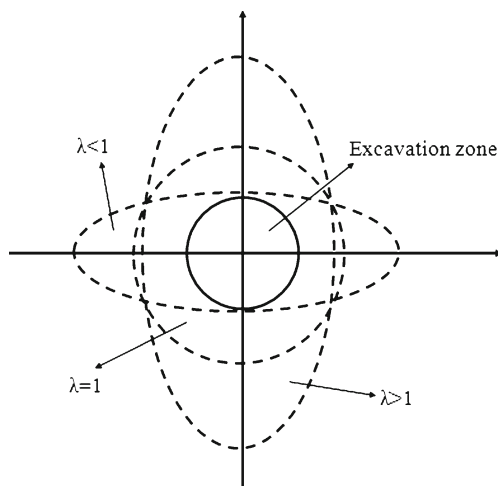
The AE characteristics recorded at a 0.0001 s interval for various lateral pressure coefficients are presented in Fig. 16.
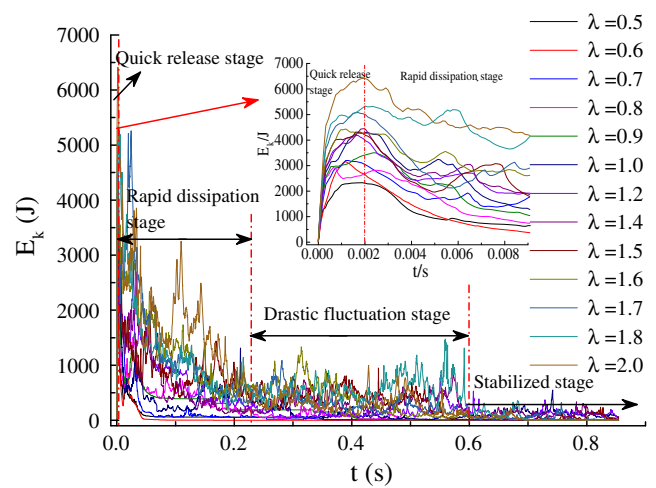
Fig. 10 Unloading deformation and stress distribution of particles around hydraulic slotting boreholes (the *grey circles* represent particles which compose the coal mass; the *black zone* points to stress concentration zone)

Fig. 12 Loaded model of an infinite plate with a circular

Fig. 14 Kinetic energy evolution with different lateral pressure coefficients (the *red arrow* points to the partial enlarged view at the point of peak value; the *black arrow* represents various stages of kinetic energy evolution)

When λ is small, such as 0.6 and 0.7, the AE events that are characterized by discrete distribution, unobvious regularity and small frequency in one event are few and occur mainly during the initial time. When λ=1, the distribution of AE events is uniform during the entire process, and an interval of distinct high-frequency AE events is not observed. When λ>1, the distribution of AE events follows an analogous and obvious rule. First, the number of AE events increases sharply after hydraulic slotting, and then undergoes a process of rapid decrease before disappearing. For λ=2.0, for example, we find that after excavation, the number of AE events declines shapely after a surge. This period lasts ~0.2 s. From 0.2 to 0.6 s, the AE events distribute uniformly. When the calculation time exceeds 0.6 s, the number of AE events is negligible. These conclusions agree well with the rules of kinetic energy evolution in Fig. 15 and verify the reasonality of the partition of kinetic energy evolution.
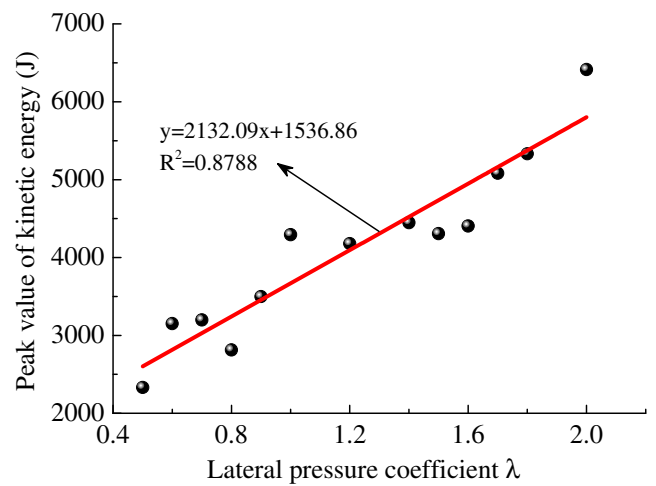
The coal mass permeability is related closely to the cracks in coal. Under the same circumstances, the permeability is in direct proportion to the crack number (Nabawy 2014; Michael and Daniel 2010; Xia et al. 2014; Yang et al. 2014; Yan et al. 2014; Zhu et al. 2014). As has been shown above, the damage zone varies with lateral pressure coefficient. The area coverage of the damage zone in the orientation of minimum principal stress is larger than that in the orientation of maximum principal stress. This means that the gas in the coal mass that distributes along the orientation of minimum principal stress around the slotted borehole will be extracted more easily. This conclusion will be of guiding significance to the layout of the gas drainage borehole.

Fig. 13 Schematic diagram of damage zone around the circle under various λ

$$y=2132.09x+1536.86$$
$$R^2=0.8788$$

Fig. 15 Relationship between the kinetic energy peak value and lateral pressure coefficient
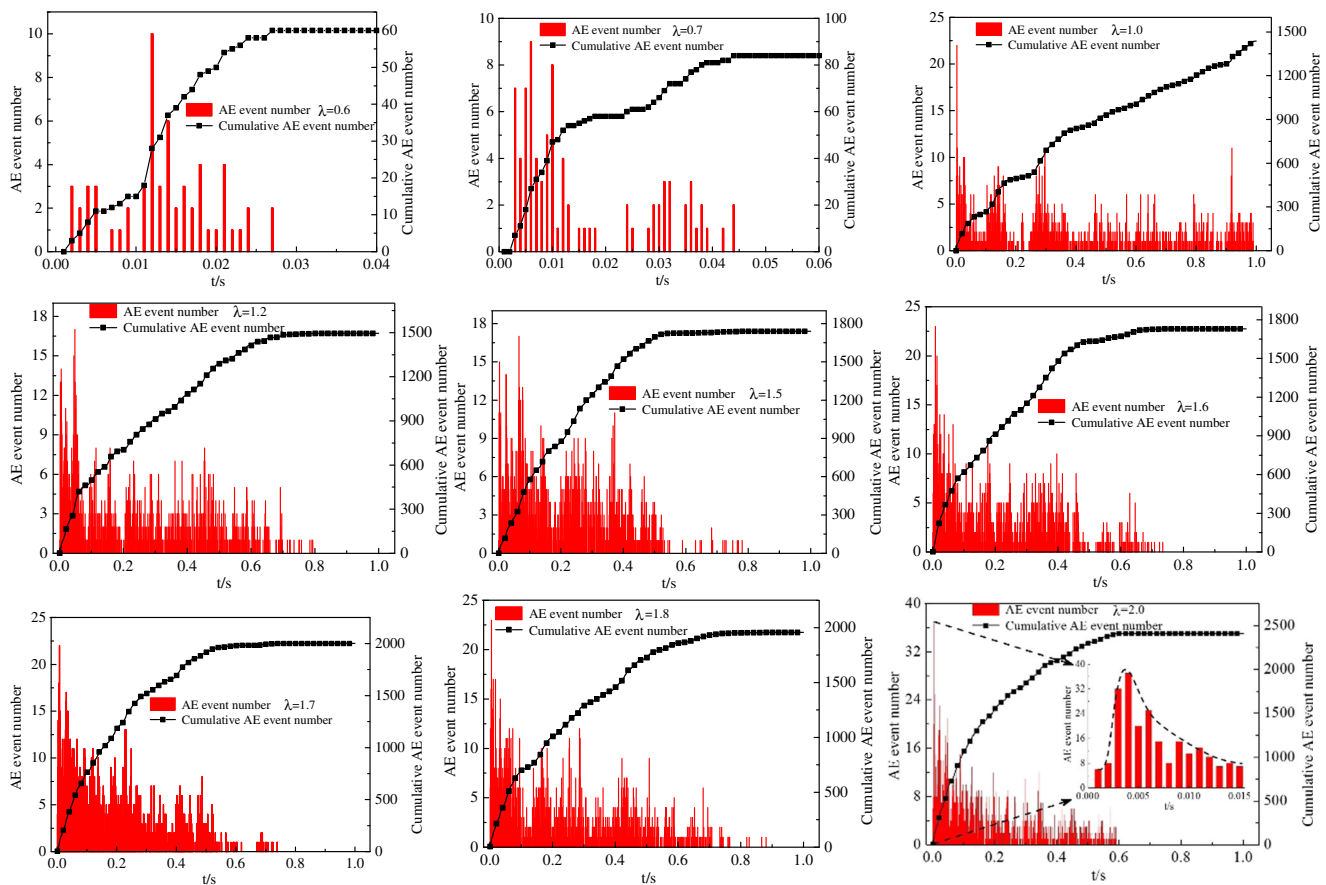
Fig. 16 Relationship between acoustic emission frequency and time

Conclusions

Crack propagation patterns, rules of kinetic energy evolution, and AE characteristics have been elaborated by PFC2D based on the DEM. Various models have been established to illustrate the effect of lateral pressure coefficient on the fracture behavior of coal around the slotted borehole. The following conclusions can be drawn:

(1) When λ<1.0, cracks propagate mainly in the horizontal direction and some in the vertical direction. The damage zone can be viewed as approximating an ellipse, the long axis of which is in the horizontal direction. While λ=1.0, the fracture zone is almost circular. If λ>1.0, cracks concentrate mainly in the vertical direction and the cracked zone can be thought of as an ellipse with long axis in the vertical direction.

(2) For the entire process, the kinetic energy evolution with various λ follows a similar rule and the time history curve of kinetic energy evolution can be divided into four stages: namely quick release, rapid dissipation, drastic fluctuation, and stabilized stages.

(3) It has been revealed that when λ is small, the AE events, which are characterized by discrete distribution, unobvious regularity, and small frequency in one event, are few and occur in initial time. While λ=1, the distribution of AE events is uniform for the entire process and an interval of distinctly high-frequency AE events is not observed. When λ>1, the distribution of AE events follows an analogous and obvious rule. The variation of AE events shows the tendency of a sharp increase before the decrease.

References

Al-Busaida, Hazzard A, Young JF et al (2005) Distinct element modeling of hydraulically fractured Lac du Bonnet granite. J Geophys Res Solid Earth 110(B6):1–14, B06302

Cai M, Kaiser PK, Morioka H et al (2007) FLAC/PFC coupled numerical simulation of AE in large-scale underground excavations. Int J Rock Mech Min Sci 44(4):550–564

Cho N, Martin CD, Sego DC (2007) A clumped particle model for rock. Int J Rock Mech Min Sci 44(7):997–1010

Cundall PA, Strack ODL (1979) A discrete numerical model for granular assemblies. Geotechnique 29:47–65

Damjanac B, Board M, Lin M et al (2007) Mechanical degradation of emplacement drifts at Yucca Mountain-A modeling case study PartII: Lithophysal rock. Int J Rock Mech Min Sci 44:368–369

Deng XF, Zhu JB, Chen SG et al (2014) Numerical study on tunnel damage subject to blast-induced shock wave in jointed rock masses. Tunn Undergr Space Technol 43:88–100

Detournay E, Peirce A (2014) On the moving boundary conditions for a hydraulic fracture. Int J Eng Sci 8:147–155

Etchells P (1997) Cutting head design lowers abrasive water jet cutting costs. Aircr Eng Aerospace Technol 69:147–150

Folkes J (2009) Waterjet—an innovative tool for manufacturing. J Mater Process Technol 209:6181–6189

Hao ZY, Zhou C, Lin BQ et al (2014) Pressure-relief and permeability-increase technology of high liquid–solid coupling blast and its application. Int J Min Sc Technol 24(1):45–49

Itasca Consulting Group Inc (2004) PFC2D (Particle Flow Code in 2 Dimensions), Version 3.1 1–1313

Iuspa L, Fusco P, Ruocco E (2015) An improved GPU-oriented algorithm for elastostatic analysis with boundary element method. Comput Struct 146:105–116

James LA (2005) Sediment from hydraulic mining detained by Englebright and small dams in the Yuba basin. Geomorphology 71:202–226

Michael J, Daniel B (2010) Fractal model for permeability calculation from porosity and pore radius information and application to excavation damaged zones surrounding waste emplacement boreholes in opalinus clay. Int J Rock Mech Min Sci 47:583–589

Kahlman L, Öjmertz KMC, Falk LKL (2001) Abrasive-waterjet testing of thermo-mechanical wear of ceramics. Wear 248:16–28

Kekec B, Kemal M, Bilim N (2014) Evaluation of the effect of vibrational wave propagation of different artificial discontinuous planes in rock samples. Arab J Geosci. doi:10.1007/s12517-014-1647-9

Kim MC, Chun HH, Kim HY et al (2009) Comparison of waterjet performance in tracked vehicles by impeller diameter. Ocean Eng 36:1438–1445

Kulekci MK (2002) Processes and apparatus developments in industrial waterjet applications. Int J Mach Tools Manuf 42:1297–1306

Li LC, Tang CA, Wang SY et al (2013) A coupled thermo-hydrologic-mechanical damage model and associated application in a stability analysis on a rock pillar. Tunn Undergr Space Technol 34:38–53

Li XB, Cao WZ, Zhou ZL et al (2014) Influence of stress path on excavation unloading response. Tunn Undergr Space Technol 42:237–246

Liang YP (2007) Study on the mechanism of coal failure by drilling of high pressure water jetting, PhD thesis, Shandong University of Science and Technology, Jinan (in Chinese)

Lin BQ, Zhang JG, Shen CM et al (2012) Technology and application of pressure relief and permeability increase by jointly drilling and slotting coal. Int J Min Sci Technol 22:545–551

Lu YY, Liu Y, Li XH, Kang Y (2010) A new method of drilling long boreholes in low permeability coal by improving its permeability. Int J Coal Geol 84:94–102

Lu TK, Zhao ZJ, Hu HF (2011) Improving the gate road development rate and reducing outburst occurrences using the water jet technique in high gas content outburst-prone soft coal seam. Int J Rock Mech Min Sci 48:1271–1282

Lu TK, Yu H, Zhou TY et al (2013) Improvement of methane drainage in high gassy coal seam using water jet technique. Int J Coal Geol 79:40–48

Mayoral JM (2014) Performance evolution of tunnels built in rigid soils. Tunn Undergr Space Technol 43:1–10

Nabawy BS (2014) Estimating porosity and permeability using digital image analysis (DIA) technique for highly porous sandstones. Arab J Geosci 7(3):889–898

Ni GH, Lin BQ, Zhai C et al (2014) Kinetic characteristics of coal gas desorption based on the pulsating injection. Int J Min Sci Technol 24(5):631–636

Park WG, Jang JH, Chun HH et al (2005) Numerical flow and performance analysis of waterjet propulsion system. Ocean Eng 32:1740–1761

Potyondy DO (2007) Simulating stress corrosion with a bonded-particle model for rock. Int J Rock Mech Min Sci 44:677–691

Potyondy DO, Cundall PA (2004) A bonded-particle model for rock. Int J Rock Mech Min Sci 41:1329–1364

Sato K, Isobe T, Mori N et al (1986) Microseismic activity associated with hydraulic mining. Int J Rock Mech Min Sci Geomech Abstr 23(1):85–94

Shanmugam DK, Nguyen T, Wang J (2008) A study of delamination on graphite/epoxy composites in abrasive waterjet machining. Compos Part A 39:923–929

Shen CM, Lin BQ, Meng FW et al (2012) Application of pressure relief and permeability increased by slotting a coal seam with a rotary type cutter working across rock layers. Int J Min Sci Technol 22:533–538

Shimizu H, Murata S, Ishida T (2011a) The distinct element analysis for hydraulic fracturing in hard rock considering fluid viscosity and particle size distribution. Int J Rock Mech Min Sci 48(5):712–727

Shimizu H, Murata S, Ishida T (2011b) The distinct element analysis for hydraulic fracturing in hard rock considering fluid viscosity and particle size distribution. Int J Rock Mech Min Sci 48:712–727

Song DZ, Wang EY, Liu ZT et al (2014) Numerical simulation of rockburst and prevention by water-jet cutting. Int J Rock Mech Min Sci 70:318–331

Tang JR, Liu YY, Ge ZL et al (2014) A new method of combined rock drilling. Int J Min Sci Technol 24:1–6

Wang XB, Pan YS (2010) Numerical simulation of rockburst processes of a circular tunnel at different lateral pressure coefficients. Rock Soil Mech 31(6):1937–1942 (in Chinese)

Wang HF, Cheng YP, Wang L (2012a) Regional gas drainage techniques in Chinese coal mines. Int J Min Sci Technol 22:873–878

Wang FT, Ren T, Tu SH et al (2012b) Implementation of underground longhole directional drilling technology for greenhouse gas mitigation in Chinese coal mines. Int J Greenhouse Gas Contr 11:290–303

Wang JG, Liu JS, Kabir A (2013) Combined effects of directional compaction, non-Darcy flow and anisotropic swelling on coal seam gas extraction. Int J Coal Geol 110:1–14

Wang L, Cheng YP, Liu HY (2014a) An analysis of fatal gas accidents in Chinese coal mines. Saf Sci 62:107–113

Wang HF, Cheng YP, Wang W et al (2014b) Research on comprehensive CBM extraction technology and its applications in China's coal mines. J Nat Gas Sci Eng 20:200–207

Wang T, Zhou WB, Chen JH et al (2014c) Simulation of hydraulic fracturing using particle flow method and application in a coal mine. Int J Coal Geol 121(1):1–13

Wu Y, Liu JS, Elsworth D et al (2010) Development of anisotropic permeability during coalbed methane production. J Nat Gas Sci Eng 2:197–210

Xia TQ, Zhou FB, Liu JS et al (2014) Evaluation of the pre-drained coal seam gas quality. Fuel 130:296–305

Yan TT, Yao YB, Liu DM et al (2014) Evaluation of the coal reservoir permeability using well logging data and its application in the Weibei coalbed methane field, southeast Ordos basin. China Arab J Geosci. doi:10.1007/s12517-014-1661-y

Yang TH, Shi WH, Wang PT et al (2014) Numerical simulation on slope stability analysis considering anisotropic properties of layered fractured rocks: a case study. Arab J Geosci. doi:10.1007/s12517-014-1609-2

Ye ZH, Chen D, Wang JG (2014) Evaluation of the non-Darcy effect in coalbed methane production. Fuel 121:1–10

Yin GZ, Qin H, Huang G et al (2012) Acoustic emission from gas-filled coal under triaxial compression. Int J Min Sci Technol 22:775–778

Yoon JS, Zang A, Stephansson O (2014) Numerical investigation on optimized stimulation of intact and naturally fractured deep geothermal reservoirs using hydro-mechanical coupled discrete particles joints model. Geothermics 52:165–184

Zhu WC, Wei CH, Liu J et al (2013) Impact of gas adsorption induced coal matrix damage on the evolution of coal permeability. Rock Mech Rock Eng 46:1353–1366

Zhu WC, Wei J, Zhao J et al (2014) 2D numerical simulation on excavation damaged zone induced by dynamic stress redistribution. Tunn Undergr Space Technol 43:315–326

Zou QL, Lin BQ, Liu T et al (2014a) Variation of methane adsorption property of coal after the treatment of hydraulic slotting and methane pre-drainage: a case study. J Nat Gas Sci Eng 20:396–406

Zou QL, Lin BQ, Liang JY et al (2014b) Variation in the pore structure of coal after hydraulic slotting and gas drainage. Adsorption Sci Technol 32:647–666